IOP Publishing | Astro Ltd Laser Physics Letters
Laser Phys. Lett. **15** (2018) 045401 (6pp) https://doi.org/10.1088/1612-202X/aaa618

Letter

Multiple nonlinear Bragg diffraction of femtosecond laser pulses in a $\chi^{(2)}$ photonic lattice with hexagonal domains

A M Vyunishev[1,2], V G Arkhipkin[1,3], I S Baturin[4,5], A R Akhmatkhanov[4,5], V Ya Shur[4,5] and A S Chirkin[6]

[1] Kirensky Institute of Physics, Federal Research Center KSC SB RAS, Krasnoyarsk, 660036, Russia
[2] Department of Photonics and Laser Technology, Siberian Federal University, Krasnoyarsk, 660079, Russia
[3] Institute of Nanotechnology, Spectroscopy and Quantum Chemistry, Siberian Federal University, Krasnoyarsk 660079, Russia
[4] School of Natural Sciences and Mathematics, Ural Federal University, Ekaterinburg 620000, Russia
[5] Labfer Ltd., Ekaterinburg 620014, Russia
[6] Faculty of Physics and International Laser Center, M. V. Lomonosov Moscow State University, Moscow 119992, Russia

E-mail: vyunishev@iph.krasn.ru

Accepted for publication 9 January 2018
Published 27 February 2018

Abstract

The frequency doubling of femtosecond laser pulses in a two-dimensional (2D) rectangular nonlinear photonic lattice with hexagonal domains is studied experimentally and theoretically. The broad fundamental spectrum enables frequency conversion under nonlinear Bragg diffraction for a series of transverse orders at a fixed longitudinal quasi-phase-matching order. The consistent nonstationary theory of the frequency doubling of femtosecond laser pulses is developed using the representation based on the reciprocal lattice of the structure. The calculated spatial distribution of the second-harmonic spectral intensity agrees well with the experimental data. The condition for multiple nonlinear Bragg diffraction in a 2D nonlinear photonic lattice is offered. The hexagonal shape of the domains contributes to multibeam second harmonic excitation. The maximum conversion efficiency for a series of transverse orders in the range 0.01%–0.03% is obtained.

Keywords: nonlinear Bragg diffraction, nonlinear photonic lattice, second harmonic generation, femtosecond pulses

(Some figures may appear in colour only in the online journal)

1. Introduction

Over the last decade, nonlinear Raman–Nath diffraction (NRND) has attracted much attention [1–7]. This phenomenon represents a series of second harmonic beams resulting from multiples of the primary reciprocal lattice vector implemented by the periodical modulation of the sign of the second-order nonlinear susceptibility of a structure in the transverse direction. Usually, the longitudinal phase-matching conditions for the NRND orders are unmet and the second-harmonic (SH)

intensity oscillates along the propagation direction, which results in a low conversion efficiency [4, 5]. As was reported in [3], the second harmonic generation (SHG) efficiency can be significantly increased by varying the angle of incidence of the fundamental frequency (FF) beam. In this case, the Cerenkov nonlinear diffraction described by the longitudinal phase matching can enhance the corresponding NRND order, which results in strong SHG under nonlinear Bragg diffraction (NBD). At the same time, it seems promising to increase the NRND by quasi-phase-matching with the use of two-dimensional (2D) nonlinear photonic lattices. They have been found to be promising for multiwavelength generation [8], the implementation of broadband parametric interactions [9], producing path-entangled photons [10] and multiple copies of beams carrying orbital angular momentum [11], and the observation of the nonlinear Talbot effect [12, 13]. Up to now, 2D nonlinear photonic lattices with periodic [14], randomized [15], superimposed [16], and chirped [17] modulation of the nonlinear susceptibility sign in the propagation direction have been investigated. Among them, only periodic structures provide a specific reciprocal lattice vector for all the NRND orders, while the phase mismatches for different orders are different. As a consequence, the respective phase mismatches are compensated at different wavelengths. This can be made by using an appropriate bandwidth of the fundamental spectrum, which is ensured by femtosecond laser pulses. In this case, NBD can take place for specific spectral components within the spectral width provided by a laser. Previously, we studied the SHG of femtosecond laser pulses under NRND and Cerenkov nonlinear diffraction in a 1D nonlinear photonic lattice [5, 18]. In [19–22], the quasi-phase-matched SHG in the continuous wave regime in 2D nonlinear photonic lattices was investigated. The frequency doubling of femtosecond laser pulses in the 2D nonlinear photonic lattice of a special design was investigated by us in [14]; however, this problem remains unsolved for 2D nonlinear photonic lattices with translational symmetry and an arbitrary domain shape.

In this Letter, we report the results of the experimental and theoretical study of the multiple SHG of femtosecond laser pulses in 2D nonlinear photonic lattices representing a rectangular lattice with hexagonal domains. The spectral width of the femtosecond pulses allows the process to be implemented under quasi-phase-matching, which results in multiple NBD at specific wavelengths. The choice of the hexagonal shape of the domains is caused by the intrinsic property of lithium niobate, where the domains have a tendency to take the form of hexagonal prisms. Moreover, the hexagonal shape of the domains provides nearly equal intensities for several SH peaks, as will be shown further.

2. Theoretical model

A 2D nonlinear photonic lattice provides a discrete set of reciprocal lattice vectors resulting in quasi-phase-matched SHG in several directions, as shown in figure 1. The spatial distribution of nonlinear susceptibility within a 2D nonlinear photonic lattice can be expressed as the series [19]

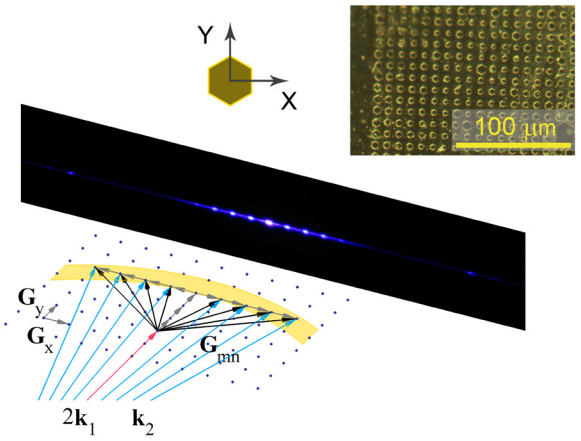

Figure 1. Far-field image of the experimental SH pattern and vectorial phase-matching diagram in reciprocal space. The reciprocal space region corresponding to the laser spectral bandwidth is colored with yellow. Inset: optical image of the etched CLN surface.

$$g(x,y) = \sum_{m,n=0,\pm1,\ldots} g_{mn} \mathrm{e}^{-\mathrm{i}(mG_x x + nG_y y)}, \tag{1}$$

where g_{mn} are Fourier coefficients, $G_{x,y} = 2\pi/\Lambda_{x,y}$ are the primitive vectors in reciprocal space (figure 1), i.e. the primitive reciprocal lattice vectors ($\Lambda_{x,y}$ is the nonlinearity modulation period along the corresponding coordinate) and n and m are the longitudinal (QPM) and transverse (NBD) orders ($m, n \in \mathbf{Z}$), respectively. For the rectangular lattice with hexagonal domains, the Fourier coefficients are (compare with [19, 20])

$$\begin{aligned} g_{mn} = {} & \mathrm{sinc}\left(m\frac{G_x\Lambda_x}{2}\right)\mathrm{sinc}\left(n\frac{G_y\Lambda_y}{2}\right) + \frac{2\sqrt{3}}{nG_y}\frac{d}{\Lambda_x\Lambda_y} \\ & \times \left\{\mathrm{sinc}\left[\frac{d}{4}(\sqrt{3}mG_x + nG_y)\right]\sin\left[\frac{d}{4}(\sqrt{3}mG_x - 3nG_y)\right]\right. \\ & \left. - \mathrm{sinc}\left[\frac{d}{4}(\sqrt{3}mG_x - nG_y)\right]\sin\left[\frac{d}{4}(\sqrt{3}mG_x + 3nG_y)\right]\right\}, \end{aligned} \tag{2}$$

where d is the hexagonal side length, $\mathrm{sinc}(x) = \sin(x)/x$.

In the quasi-optical approach, the SH field evolution inside the structure under the slowly varying amplitude approximation in the low-conversion regime is governed by the equation [23]

$$\begin{aligned} & \left(\frac{\partial}{\partial y} + \frac{1}{u_2}\frac{\partial}{\partial t}\right)A(t,r,y) + \frac{\mathrm{i}}{2k_2}\left(\frac{\partial^2}{\partial x^2} + \frac{\partial^2}{\partial z^2}\right)A(t,r,y) \\ & \quad = \Gamma g(x,y)F_r^2(r)F_t^2\left(t - \frac{y}{u_1}\right)\mathrm{e}^{\mathrm{i}\Delta k y}, \end{aligned} \tag{3}$$

where $\Delta k = k_2 - 2k_1$, $\Gamma = -\mathrm{i}\beta_2 I_1$, $\beta_2 = 2\pi k_2 \chi^{(2)}/n_2^2$, I_1 is the FF intensity at the beam center, and u_2 is the SH group velocity. For the Gaussian distribution of intensity in the time and transverse coordinates, the functions $F_t^2(t)$ and $F_r^2(r)$ take the forms

$$\begin{cases} F_r^2(r) = \exp\left(-2r^2/a^2\right) \\ F_t^2(t) = \exp\left(-2(t - y/u_1)^2/\tau^2\right). \end{cases}$$

Here, u_1 is the FF group velocity and 2τ and $2a$ are the pulse duration and the focal spot diameter of the FF beam, respectively.

The solution of (3) can be presented in the form

$$\begin{aligned} &A(\Omega, K_x, K_y, K_z, y) \\ &= \alpha y \sum_{mn} g_{mn} \exp\left(-\frac{a^2}{8}\left[(K_x + mG_x)^2 + K_z^2 + \frac{\Omega^2\tau^2}{a^2}\right]\right) \\ &\times \operatorname{sinc}\left(\frac{y}{2}\left[\Delta k + \nu\Omega - \frac{K_x^2}{2k_2} + nG_y\right]\right) \\ &\times \exp\left(\frac{\mathrm{i}y}{2}\left[\Delta k - \left(\frac{1}{u_2} + \frac{1}{u_1}\right)\Omega + \frac{K_x^2}{2k_2} + nG_y\right]\right), \end{aligned} \tag{4}$$

where $\alpha = \Gamma\tau a^2(\pi/2)^{3/2}$, $\nu = 1/u_2 - 1/u_1$ is the group velocity mismatch, $\Omega = 2\pi c(1/\lambda_2 - 2/\lambda_0)$ is the frequency detuning from the central double frequency, λ_0 is the central FF wavelength, λ_2 is the SH spectral component, and K_x and K_z are spatial frequencies. It is worth noting that in the stationary regime ($u_{1,2} \to \infty$) (4) is reduced to the form [21]. Additionally, the derived expression (4) can be implemented for the calculation of SHG in 2D rectangle nonlinear photonic lattices with an arbitrary domain shape. The requirement is to specify the Fourier coefficients g_{mn}.

Consider the spectral density for fixed values of m and n at a distance $y = L$

$$\begin{aligned} &S_{mn}(\Omega, K_x, K_y, y = L) = |A_{mn}(\Omega, L)|^2 \\ &= (\alpha g_{mn} L)^2 \exp\left[-\frac{(\tau\Omega)^2}{4} - \frac{a^2}{4}(K_x + mG_x)^2\right] \\ &\exp\left[-0.09\left(\Delta k + \nu\Omega - \frac{K_x^2}{2k_2} + nG_y\right)L\right]. \end{aligned} \tag{5}$$

Here the substitution $\operatorname{sinc}^2(\xi) \to \exp(0.36\xi^2)$ is used [23] and $K_z = 0$. The first exponent in (5) defines the angular positions of SH spectral maxima, which are given by condition $K_x + mG_x = 0$. When the QPM is introduced in the longitudinal direction, i.e. when the condition

$$\Delta k + \nu\Omega - \frac{K_x^2}{2k_2} + nG_y = 0 \tag{6}$$

is fulfilled, NBD occurs.

Analysis of (5) shows that the spectral position of the NBD order $\{m,n\}$ can be determined as

$$\Omega_{mn} = \nu^{-1}\left(\frac{Q}{2L}m^2 - \frac{2\pi}{\Lambda_y}n - \Delta k\right). \tag{7}$$

Here $Q = 2\pi\lambda_2 L/n_2\Lambda_x^2$. It can be seen that Ω_{mn} obeys quadratic law on the transverse order m. The first term in (6) increases slower than the second one at not very large values of Q as $L \gg \Lambda_y$ or, since $\lambda_2/\Lambda_x \ll 1$, in the largest of all the experimental implementations. It means also that the spectral intervals between the adjacent orders m are smaller than the spectral intervals between the orders n. Using (6), we find the required lattice period in the longitudinal direction in order to obtain the multiple quasi-phase-matched SHG at a given wavelength.

The spectral interval between the peak orders $m + 1$ and m is

$$\Delta\lambda_m = \frac{(1 + 2|m|)\lambda_2^3}{2n_2 c|\nu|\Lambda_x^2} = \frac{(1 + 2|m|)\lambda_2^2 Q}{4\pi c|\nu|L}. \tag{8}$$

Multiple NBD orders are observed when $\Delta\lambda/\Delta\lambda_m \gg 1$ ($\Delta\lambda$ is the FF spectral width).

The spectral interval between the adjacent orders $n + 1$ and n is

$$\Delta\lambda_n = \frac{\lambda_2^2}{c|\nu|\Lambda_y}. \tag{9}$$

Note that $\Delta\lambda_n$ is independent of the order n and amounts approximately to 40 nm under the experimental conditions. The spectral width of an arbitrary order $\{m, n\}$ can be found as

$$\delta\lambda_{mn} \approx 2\sqrt{\ln 2}\frac{\lambda_2^2}{c|\nu|L}. \tag{10}$$

Let us define the SH power in the NBD order $\{m, n\}$ at the frequency Ω_{mn} so that $P_{mn} = P(\Omega_{mn}; L)$, which is governed by

$$\begin{aligned} P_{mn} &\approx \int_{-\infty}^{\infty} S_{mn}(\Omega = \Omega_{mn} + \delta\Omega; L)\mathrm{d}\delta\Omega \\ &= \frac{2\sqrt{\pi}(\alpha g_{mn} L)^2}{\tau\sqrt{1 + (\tau_d/\tau)^2}} \exp\left[-\frac{(\tau_d/\tau)^2}{4(1 + (\tau_d/\tau)^2)}(\tau\Omega_{mn})^2\right], \end{aligned} \tag{11}$$

where $\tau_d = 0.6|\nu|L$ is the group delay time. Then, the ratio between SH powers $\eta = P_{m_1n_1}/P_{m_2n_2}$ for different pairs $\{m,n\}$ under the condition $\tau_d \gg \tau$ is

$$\eta = \left(\frac{g_{m_1n_1}}{g_{m_2n_2}}\right)^2 \frac{2\sqrt{\pi}}{\tau_d} \exp\left[-\frac{1}{4}\tau_d^2(\Omega_{m_1n_1}^2 - \Omega_{m_2n_2}^2)\right]. \tag{12}$$

If the factor of the exponent in (12) is smaller than unity, the ratio between SH powers is determined as the squared ratio between the 2D Fourier coefficients of the nonlinear photonic lattice.

3. Results and discussion

In the experiment, we used a congruent lithium niobate-based nonlinear photonic lattice. The nonlinear photonic lattice structure was fabricated by electric field poling (Labfer Ltd) [24]. The sample size was $5.0 \times 2.0 \times 0.5$ mm^3 ($x \times y \times z$). The square lattice period was about $\Lambda_{x,y} = 10$ μm. Each lattice point contains domains with a nearly hexagonal shape (see the inset in figure 1). Two of the hexagonal domain sides were parallel to the y axis of the crystal. The measured hexagonal side length d was measured to be $\sim 0.29\Lambda_x$. In the experiments, the FF beam from a Spectra-Physics Tsunami Ti:sapphire oscillator delivering 85 fs pulses at a repetition rate of 80 MHz was focused onto the sample by a 20 cm lens to produce a beam with a focal diameter of $2a = 136$ μm (confocal parameter 3.4 cm). The fundamental radiation propagated along the y axis and its polarization coincided with the z axis to employ the highest nonlinear coefficient of lithium niobate d_{33}. The central fundamental wavelength

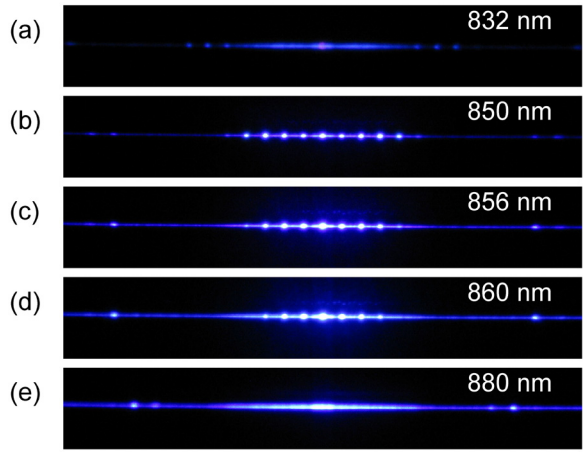

Figure 2. Far-field image of the experimental SH pattern on a central FF wavelength.

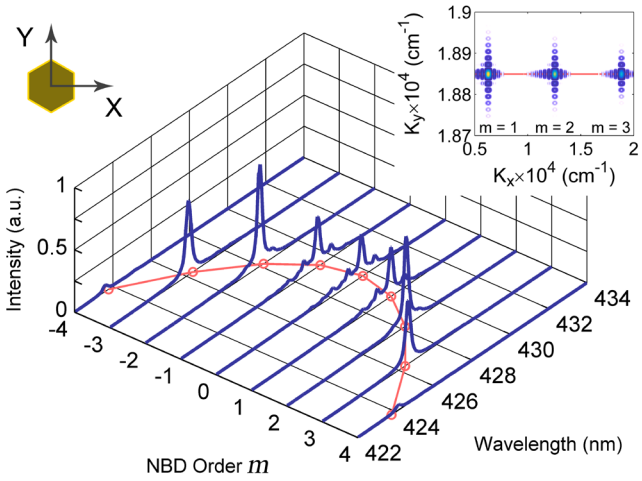

Figure 3. Measured SH spectra and SH peak wavelengths (red points) for the NBD orders. Inset: Fourier spectrum of the structure under study (the red solid line indicates the value $K_y = 3G_y$).

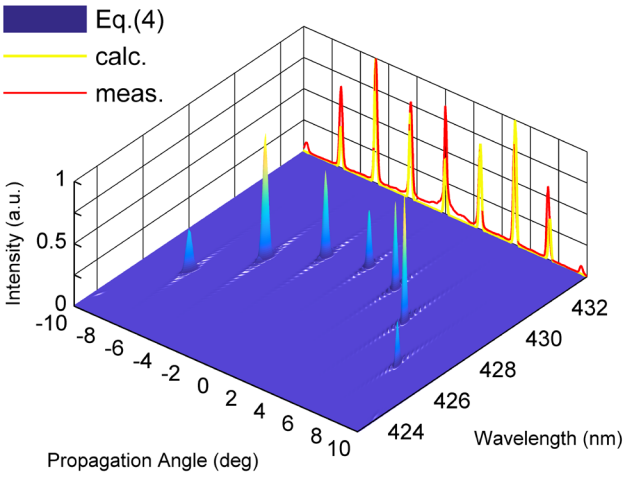

Figure 4. Angular dependence of the SH spectral intensity calculated using (4), and the calculated and measured angular dependences of the SH intensity.

was scanned from 830–880 nm to obtain multiple SHG under NBD. Figure 2 shows the SH far-field images observed on a screen at a distance of 7 cm from the sample for a set of the central fundamental wavelengths. NBD is clearly observed at the wavelengths 850–860 nm (figures 2(b)–(d)). At the central fundamental wavelength, 856 nm is chosen as an optimal wavelength since the maximum SHG efficiency is achieved for a larger number of transverse orders m in this case (figure 2(c)). Therefore, in the following experiments, the central fundamental wavelength was tuned to a wavelength of 856 nm to implement the 3rd order quasi-phase-matching for the 2nd transverse order (the NBD order $\{2,3\}$).

The SH spectra were measured by an MSDD 1000 spectrometer (TII, Solar) with a spectral resolution of 0.02 nm. It can be seen in figure 3 that the SH spectra consist of a single peak that undergoes a short-wavelength spectral shift with increasing order. Moreover, the central peak is surrounded by secondary maxima for $m = 0$ and $m = \pm 1$. According to the Fourier analysis of the structure (see the inset in figure 3), the secondary maxima originate from the periodic modulation of nonlinearity in the structure. The hexagonal shape of the domains is analyzed to provide a nearly equal distribution of intensity between the NBD orders. In addition, a background appears in the spectral intensity, which can be attributed to random variations in the domain size (figure 3).

The angular dependence of the SH spectral intensity ($S_2(\Omega, K) = |A(\Omega, K, L)|^2$) calculated using (4) is shown in figure 4. Good agreement between the calculated dependence and measured SH spectra is achieved under the following parameters: the sample length $L = 2$ mm, the hexagonal side length $d = 2.9$ μm, the central FF wavelength 856.4 nm, the pulse duration $2\tau = 144$ fs, the focal spot diameter $2a = 136$ μm. The required refractive index data were taken from [25]. The approach proposed allows us to not only describe the angular distribution of the spectral intensity, but also to evaluate the spectral and angular widths of the SH peaks for specific NBD orders. Additionally, the calculated dependence demonstrates the short-wavelength spectral shift of maxima with increasing NBD order m according to (7). Unlike the calculated angular dependence of the spectral intensity, the measured SH spectra are broader, which can be attributed to the fluctuation of the hexagonal domain sizes. The angular distribution of the SH intensity integrated over the spectrum is shown in the same figure in comparison with the measured dependence obtained by translating the narrow width slit in the transverse direction. For this purpose, a Newport 918D power meter was also used.

Table 1. Calculated ((10) and (8)) and experimental spectral widths ($\delta\lambda_m$) and intervals ($\Delta\lambda_m$). The brackets $\langle ... \rangle$ indicate the average value.

m	λ_m (nm)	$\delta\lambda_m$ (nm)	$\Delta\lambda_m$ (nm)	$\langle\lambda_m^{\mathrm{exp}}\rangle$ (nm)	$\langle\delta\lambda_m^{\mathrm{exp}}\rangle$ (nm)	$\langle\Delta\lambda_m^{\mathrm{exp}}\rangle$ (nm)
0	429.7	0.33	—	429.6	0.2	—
±1	429.3	0.33	0.37	429.3	0.2	0.3
±2	428.2	0.33	1.12	428.1	0.3	1.2
±3	426.3	0.33	1.85	426.3	0.3	1.8
±4	423.8	0.33	2.56	423.8	0.4	2.5

The SH peak wavelengths (λ_m), spectral widths ($\delta\lambda_m$), and intervals ($\Delta\lambda_m$) were calculated using (8), (9) and (10), respectively. These values for $m \in [-4, 4]$ are given in table 1. In

addition, table 1 summarizes the average measured SH peak wavelengths, spectral widths, and intervals. The measurement accuracy of the spectral characteristics was about 0.02 nm. It can be seen that the calculated values are in good agreement with the measured ones.

As can be seen in figure 1, the central spots corresponding to the NBD are brighter than the side spots corresponding to Cerenkov nonlinear diffraction [14]. The measured maximum conversion efficiency for a series of transverse orders (central spots) lies in the range 0.01%–0.03% , which is higher than the value obtained in our previous work [14] by a magnitude of about 20. Let us introduce the structure gain coefficient as a ratio of employed longitudinal orders n and structure lengths L, i.e. $(n_1L_2/n_2L_1)^2$, where the indexes 1,2 are related to the previous [14] and current study, respectively. For $m = \pm 1$, the calculation gives the structure gain coefficient $\sim$18, which agrees with our measurements.

Usually, acousto optics distinguishes the two diffraction regimes: Raman–Nath and Bragg. The criterion of the diffraction regime is the Klein–Cook parameter Q_{KC} [26]. At $Q_{KC} \gg 1$, the Bragg diffraction takes place; otherwise, Raman–Nath diffraction is observed ($Q_{KC} < 1$). Assuming that the diffraction phenomena has the same nature, we have introduced a similar parameter to distinguish the nonlinear diffraction regime. In our model, it is parameter Q in (6). Calculations yield a value of $Q \approx 24$, which indicates the Bragg nonlinear diffraction regime.

4. Conclusion

Thus, the frequency doubling of femtosecond laser pulses in a 2D rectangular nonlinear photonic lattice with hexagonal domains was studied. It was shown that the broad fundamental spectrum enables frequency conversion under the NBD for five transverse orders with the efficiency varying from 0.01%– to 0.03%, which is higher than the value obtained in our previous work by a magnitude of about 20. The consistent nonstationary theory of the frequency doubling of femtosecond laser pulses was developed, which uses the representation based on the reciprocal lattice of the structure. The condition for NBD in a 2D nonlinear photonic lattice is suggested. The calculated spatial distribution of the SH spectral intensity agrees well with the experimental data.

Acknowledgments

The work was supported by the Russian Foundation for Basic Research through grant 15-02-03838. ISB, ARA and VYS acknowledge the support of the Government of the Russian Federation (Act 211, Agreement 02.A03.21.0006).

References

[1] Saltiel S M, Neshev D N, Fischer R, Krolikowski W, Arie A and Kivshar Y S 2008 Generation of second-harmonic conical waves via nonlinear Bragg diffraction *Phys. Rev. Lett.* **100** 103902

[2] Saltiel S M, Neshev D N, Krolikowski W, Arie A, Bang O and Kivshar Y S 2009 Multiorder nonlinear diffraction in frequency doubling processes *Opt. Lett.* **34** 848–50

[3] Kalinowski K, Roedig P, Sheng Y, Ayoub M, Imbrock J, Denz C and Krolikowski W 2012 Enhanced Cerenkov second-harmonic emission in nonlinear photonic structures *Opt. Lett.* **37** 1832–4

[4] Sheng Y, Kong Q, Wang W, Kalinowski K and Krolikowski W 2012 Theoretical investigations of nonlinear Raman–Nath diffraction in the frequency doubling process *J. Phys. B: At. Mol. Opt. Phys.* **45** 055401

[5] Vyunishev A M, Slabko V V, Baturin I S, Akhmatkhanov A R and Shur V Y 2014 Nonlinear Raman–Nath diffraction of femtosecond laser pulses *Opt. Lett.* **39** 4231–4

[6] Liu H, Li J, Zhao X, Zheng Y and Chen X 2016 Nonlinear Raman–Nath second harmonic generation with structured fundamental wave *Opt. Express* **24** 15666–71

[7] Zhou H, Liu H, Sang M, Li J and Chen X 2017 Nonlinear Raman–Nath second harmonic generation of hybrid structured fundamental wave *Opt. Express* **25** 3774–9

[8] Yellas Z, Lee M W, Kremer R, Chang K-H, Beghoul M R, Peng L-H and Boudrioua A 2017 Multiwavelength generation from multi-nonlinear optical process in a 2D PPLT *Opt. Express* **25** 30253–8

[9] Conforti M, Baronio F, Levenius M and Gallo K 2014 Broadband parametric processes in $\chi^{(2)}$ nonlinear photonic crystals *Opt. Lett.* **39** 3457–60

[10] Megidish E, Halevy A, Eisenberg H S, Ganany-Padowicz A, Habshoosh N and Arie A 2013 Compact 2D nonlinear photonic crystal source of beamlike path entangled photons *Opt. Express* **21** 6689–96

[11] Fang X, Wei D, Liu D, Zhong W, Ni R, Chen Z, Hu X, Zhang Y, Zhu S N and Xiao M 2015 Multiple copies of orbital angular momentum states through second-harmonic generation in a two-dimensional periodically poled $LiTaO_3$ crystal *Appl. Phys. Lett.* **107** 161102

[12] Zhang Y, Wen J, Zhu S N and Xiao M 2010 Nonlinear Talbot effect *Phys. Rev. Lett.* **104** 183901

[13] Wei D, Liu D, Hu X, Zhang Y and Xiao M 2014 Superposed second-harmonic Talbot self-image from a PPLT crystal *Laser Phys. Lett.* **11** 095402

[14] Vyunishev A M, Arkhipkin V G, Slabko V V, Baturin I S, Akhmatkhanov A R, Shur V Y and Chirkin A S 2015 Nonlinear Raman–Nath diffraction of femtosecond laser pulses in a 2D nonlinear photonic crystal *Opt. Lett.* **40** 4002–5

[15] Wang W W, Sheng Y, Roppo V, Chen Z, Niu X and Krolikowski W 2013 Enhancement of nonlinear Raman–Nath diffraction in two-dimensional optical superlattice *Opt. Express* **21** 18671–9

[16] Vyunishev A M and Chirkin A S 2015 Multiple quasi-phase-matching in nonlinear Raman–Nath diffraction *Opt. Lett.* **40** 1314–7

[17] Vyunishev A M, Arkhipkin V G and Chirkin A S 2015 Theory of second-harmonic generation in a chirped 2D nonlinear optical superlattice under nonlinear Raman–Nath diffraction *J. Opt. Soc. Am.* B **32** 2411–6

[18] Vyunishev A M, Aleksandrovsky A S, Zaitsev A I and Slabko V V 2013 Čerenkov nonlinear diffraction of femtosecond pulses *J. Opt. Soc. Am.* B **30** 2014–21

[19] Arie A, Habshoosh N and Bahabad A 2007 Quasi phase matching in two-dimensional nonlinear photonic crystals *Opt. Quantum Electron.* **39** 361–75

[20] Arie A, Bahabad A and Habshoosh N 2009 Nonlinear interactions in periodic and quasi-periodic nonlinear photonic crystals *Ferroelectric Crystals for Photonic Applications: Including Nanoscale Fabrication and Characterization Techniques* ed P Ferraro *et al* (Berlin: Springer)

[21] Sheng Y, Roppo V, Kong Q, Kalinowski K, Wang Q, Cojocaru C, Trull J and Krolikowski W 2011

Tailoring Cerenkov second-harmonic generation in bulk nonlinear photonic crystal *Opt. Lett.* **36** 2593–5

[22] Li J, Li Z and Zhang D 2007 Effects of shapes and orientations of reversed domains on the conversion efficiency of second harmonic wave in two-dimensional nonlinear photonic crystals *J. Appl. Phys.* **102** 093101

[23] Shutov I V, Ozheredov I A, Shumitski A V and Chirkin A S 2008 Second harmonic generation by femtosecond laser pulses in the Laue scheme *Opt. Spectrosc.* **105** 79–84

[24] Shur V Y 2006 Kinetics of ferroelectric domains: application of general approach to $LiNbO_3$ and $LiTaO_3$ *J. Mater. Sci.* **41** 199–210

[25] Jundt D H 1997 Temperature-dependent Sellmeier equation for the index of refraction, n_e, in congruent lithium niobate *Opt. Lett.* **22** 1553–5

[26] Kwiek P, Molkenstruck W and Reibold R 1996 Determination of the Klein–Cook parameter in ultrasound light diffraction *Ultrasonics* **34** 801–5